The Astrophysical Journal, 650:438–450, 2006 October 10

SOLAR SOURCES OF IMPULSIVE SOLAR ENERGETIC PARTICLE EVENTS AND THEIR MAGNETIC FIELD CONNECTION TO THE EARTH

Nariaki V. Nitta,[1] Donald V. Reames,[2] Marc L. DeRosa,[1] Yang Liu,[3]
Seiji Yashiro,[4] and Natchimuthuk Gopalswamy[5]
Received 2006 March 14; accepted 2006 June 27

ABSTRACT

This paper investigates the solar origin of impulsive solar energetic particle (SEP) events, often referred to as ^{3}He-rich flares, by attempting to locate the source regions of 117 events as observed at ~2–3 MeV amu^{-1}. Given large uncertainties as to when ions at these energies were injected, we use type III radio bursts that occur within a 5 hr time window preceding the observed ion onset, and search in EUV and X-ray full-disk images for brightenings around the times of the type III bursts. In this way we find the solar sources in 69 events. High cadence EUV images often reveal a jet in the source region shortly after the type III burst. We also study magnetic field connections between the Earth and the solar sources of impulsive SEP events as identified above, combining the potential field source surface (PFSS) model for the coronal field and the Parker spiral for the interplanetary magnetic field. We find open field lines in and around ~80% of the source regions. But only in ~40% of the cases, can we find field lines that are both close to the source region at the photosphere and to the Parker spiral coordinates at the source surface, suggesting challenges in understanding the Sun-Earth magnetic field with observations available at present and in near future.

Subject headings: Sun: flares — Sun: magnetic fields — Sun: particle emission — Sun: X-rays, gamma rays

1. INTRODUCTION

Solar energetic particle (SEP) events are often divided into two classes, gradual and impulsive, on the basis of their properties such as the abundances and charge states (Reames 1999). Gradual SEP events, which can be so intense as to present a space weather threat, are characterized by the abundances and charge states of solar wind, whereas impulsive SEP events have high charge states and enrichment in certain ion species relative to coronal values (e.g., enrichment of ~10 in Fe/O, and ~1000 in ^{3}He/^{4}He and hence the nomenclature of "^{3}He-rich flares"). It has been shown (e.g., Kahler et al. 1984) that gradual SEP events are almost always accompanied by fast and wide coronal mass ejections (CMEs), suggesting their origin at CME-driven shocks. In contrast, the poor correlation of impulsive SEP events with CMEs (Kahler et al. 1985) has been used as an argument to seek their origin in impulsive solar flares, which are often thought to be distinct from long-duration flares characteristic of energetic CMEs (Pallavicini et al. 1977; Kahler et al. 1989, but also see Nitta & Hudson 2001 for exceptional cases).

The view of impulsive solar flares as solar sources of impulsive SEP events has not yet been convincingly supported by observations. In other words, we still do not know if impulsive solar flares at well-connected regions always result in ^{3}He-rich SEP events. Limited studies on the solar sources of impulsive SEP events (Kahler et al. 1987; Reames et al. 1988) failed to see a characteristic pattern of the associated solar flares; sometimes no solar flares were found. Instead, past studies have shown that ^{3}He-rich SEP events are correlated with 2–100 keV electron events (Reames et al. 1985) and kilometric (and metric) type III radio bursts (Reames & Stone 1986).

It has recently been suggested (Krucker et al. 1999; Haggerty & Roelof 2002), however, that at least the high-energy ($\gtrsim$30 keV) part of electron events is often better associated with CMEs or CME-associated coronal waves, because these particles appear to be released closer in time to them than to the associated type III bursts, although low-energy electrons may be released closer in time to type III bursts (Wang et al. 2005). Furthermore, (metric) type III radio bursts have been shown to be poorly correlated with solar flares as seen in hard X-rays (Kane 1981). This is probably because a majority of solar flares occur in closed magnetic field configurations. Connections of type III bursts with solar flares would be even weaker if we include those that start at longer wavelengths (i.e., higher altitudes).

To further complicate the issue, impulsive SEP events are now more frequently associated with CMEs (Kahler et al. 2001; Yashiro et al. 2004) than previously shown (Kahler et al. 1985). The increased CME association presumably results from the significantly increased sensitivity of the Large Angle and Spectrographic Coronagraph (LASCO; Brueckner et al. 1995) on the *Solar and Heliospheric Observatory* (*SOHO*).

One of the reasons that we still do not clearly understand the origin of impulsive SEP events may be that solar images have not been regularly used in such studies. The EUV and X-ray images greatly help us identify minor brightenings that may be associated with impulsive SEP events, but are not intense enough to be seen in *GOES* (*Geostationary Operational Environmental Satellite*) light curves or to be included in flare lists based on Hα patrol observations. Flares associated with impulsive SEP events tend to be small, and the ^{3}He/^{4}He is anticorrelated with the intensity of the associated flares (Reames et al. 1988). Recently, Wang et al. (2006) have proposed that jets seen in EUV and sometimes in white-light images (Wang & Sheeley 2002) be the solar sources of impulsive SEP events without their explicit reference to impulsive solar flares. They analyzed images from the EUV Imaging Telescope (EIT; Delaboudinière et al. 1995) and LASCO

[1] Lockheed Martin Solar and Astrophysics Laboratory, Department/ADBS, B/252, 3251 Hanover Street, Palo Alto, CA 94304; nitta@lmsal.com, derosa@lmsal.com.
[2] NASA Goddard Space Flight Center, Code 661, Greenbelt, MD 20771; reames@milkyway.gsfc.nasa.gov.
[3] W. W. Hansen Experimental Laboratory, 455 via Palou, Stanford University, Stanford, CA 34305; yliu@quake.stanford.edu.
[4] The Catholic University of America, Washington, DC 20064; yashiro@ssedmail.gsfc.nasa.gov.
[5] NASA Goddard Space Flight Center, Code 695, Greenbelt, MD 20771; gopals@ssedmail.gsfc.nasa.gov.

around the estimated injection times of 25 ^{3}He-rich events. This result may be expected from the association of X-ray jets with type III bursts (e.g., Kundu et al. 1995). According to Wang et al. (2006), these jets are located at the interface between active regions and adjacent open field regions, which are both identified in He I λ10830 Å images as less dark areas, and shown by the potential field source surface (PFSS) magnetic field model (Schatten et al. 1969). An important question we may ask, however, is if the PFSS model reliably gives Earth-directed open field lines in small coronal holes, typically observed during cycle maximum, which are not as clearly seen in images or long-lived as extended coronal holes.

In this paper we study the solar sources of impulsive SEP events in a larger sample, examining full-disk images obtained by EIT and the *Yohkoh* Soft X-Ray Telescope (SXT; Tsuneta et al. 1991). Rather than explicitly searching for jets in a limited range of longitudes, we use decametric-hectometric (DH) type III bursts to narrow down the times at which we locate flares or brightenings in the low corona that may be linked with acceleration of impulsive SEPs. We describe our analysis in § 2, and give the result of source identification in § 3. Using the solar sources thus identified, we then compare these source locations with the footpoints of the magnetic field lines that are calculated to intersect the Earth, using the PFSS model for the corona and the Parker spiral for the interplanetary space (§ 4). In § 5, we discuss our results, including the caveat of the PFSS model in understanding the magnetic field connection between the Earth and the source regions of impulsive SEP events. We give a summary in § 6.

2. OBSERVATIONS

We selected a total of 117 impulsive SEP events between 1994 December and 2002 December in data from the Low-Energy Matrix Telescope (LEMT), which is part of the Energetic Particles: Acceleration, Composition, and Transport (EPACT; von Rosenvinge et al. 1995) experiment on board the *Wind* spacecraft. Our selection criteria was based on ^{3}He/^{4}He and Fe/O in the 2–3 MeV amu^{-1} range. We group the events into three categories: category 1 if ^{3}He/^{4}He > 0.5 and Fe and O are unobserved, category 2 if Fe/O > 0.5 and ^{3}He/^{4}He < 0.5 or ^{3}He is below the background of ^{4}He, and category 3 if ^{3}He/^{4}He > 0.5 and Fe/O > 0.5. Most of these events have a clear velocity dispersion, suggesting a new injection at the Sun. Subsets of these events have been studied in the context of the association of impulsive SEP events with CMEs and type II radio bursts (Yashiro et al. 2004) and the enhancement of ultraheavy elements (Reames & Ng 2004). Our master list includes 12 of the 25 events studied by Wang et al. (2006), who used SEP data at somewhat lower energies.

2.1. *Ion Injection Times*

The ion onset time, as observed by LEMT, can usually be determined to within an hour. In principle, we could calculate when ions were injected and released from the Sun, given the observed energies and a typical path length of field lines in the Parker spiral (e.g., 1.2 AU.) However, we should keep in mind the random walk nature of the heliospheric magnetic field lines (e.g., Jokipii & Parker 1969; Ragot 1999); the effect of scattering may not be negligible, effectively increasing the uncertainties in the path length. Alternatively, we could extrapolate the velocity dispersion of ions and calculate both the ion release time and the path length, assuming that first-arriving particles are scatter-free. But the results may be equally uncertain due to limited ranges of velocity and to poor statistics. Furthermore, recent studies (Lintunen & Vainio 2004; Sáiz et al. 2005) have pointed out problems with the scatter-free assumption commonly employed in such analyses.

TABLE 1
Association of Impulsive SEP Events with Other Signatures

Category[a]	Type III	Electrons	CMEs
1	35/38	11/38	7/20
2	30/31	21/30	19/26
3	45/47	36/42	20/29
Total	110/116	68/110	46/75

[a] 1 if ^{3}He/^{4}He >0.5, and Fe and O are unobserved, 2 if Fe/O > 0.5, and ^{3}He/^{4}He < 0.5 or ^{3}He is below background ^{4}He, and 3 if ^{3}He/^{4}He > 0.5 and Fe/O > 0.5.

Instead, we use known proxies for impulsive SEP events that may provide injection times with less uncertainty. It has been shown that ^{3}He-rich SEP events are correlated with type III bursts (Reames & Stone 1986), and with 2–100 keV electron events (Reames et al. 1985). In particular, the timings of type III bursts, known to the accuracy of a minute, can be directly compared with the timings of flares as observed at EUV and X-ray wavelengths. Type III bursts are found in data from the Radio and Plasma Wave Experiment (WAVES; Bougeret et al. 1995) on *Wind*, which produces radio dynamic spectra between 13.8 MHz and 4 kHz.

We first search for type III bursts in WAVES data in a 5 hr time window preceding the observed ion onset. This may seem too long a window, since 2 MeV amu^{-1} particles take only 2.5 hr to travel the typical path length of 1.2 AU, but we do not assume that first-arriving ions are scatter free. As shown in Table 1, at least one type III burst is found in the 5 hr window for 110 of 116 impulsive SEP events; one event in the original list has poor WAVES data. In many cases, we find multiple type III bursts in this time window. Higher preference is given to intense type III bursts that extend to frequencies as low as the local plasma frequency at the spacecraft, typically $\lesssim$50 kHz, because they are more likely to be associated with SEPs at 1 AU. For a better connection to the solar source, the type III signal at $\gtrsim$10 MHz is also considered to be an important factor.

Another criterion for distinguishing multiple type III bursts is the occurrence of an electron event (Reames et al. 1985). We use >30 keV electron data from the Three-dimensional Plasma and Energetic Particles instrument (3DP; Lin et al. 1995) also on *Wind*. The frequency of >30 keV electron events in the 5 hr window is much lower ($\sim$60%) than that of type III bursts (Table 1). This number is likely to be an overestimate for electron events of solar origin, since we include all the electron events irrespective of the time difference from a type III burst and the pitch angle distribution; the detailed properties of the electron events are beyond the scope of this study. When multiple type III bursts look much the same, we can use images (§ 2.2) to locate each of them. If they come from different regions, we designate the event as ambiguous and exclude it from further study. On the other hand, the multiple type III bursts in a short period often correspond to brightenings at the same region.

Figure 1 shows an example of three impulsive SEP events and their associated signatures. In each of events 1–3, it is not difficult to choose the type III burst that we associate with impulsive SEP events, primarily because of the accompanying electron event. For event 2, we note three type III bursts, all of which are associated with an electron event. Images show that these type III bursts are associated with brightenings in the same region, presumably corresponding to multiple injections of particles. More challenging examples are given in Figure 2. None of these impulsive SEP events, typically in category 1, were preceded by an electron event. Moreover, the only prominent type III

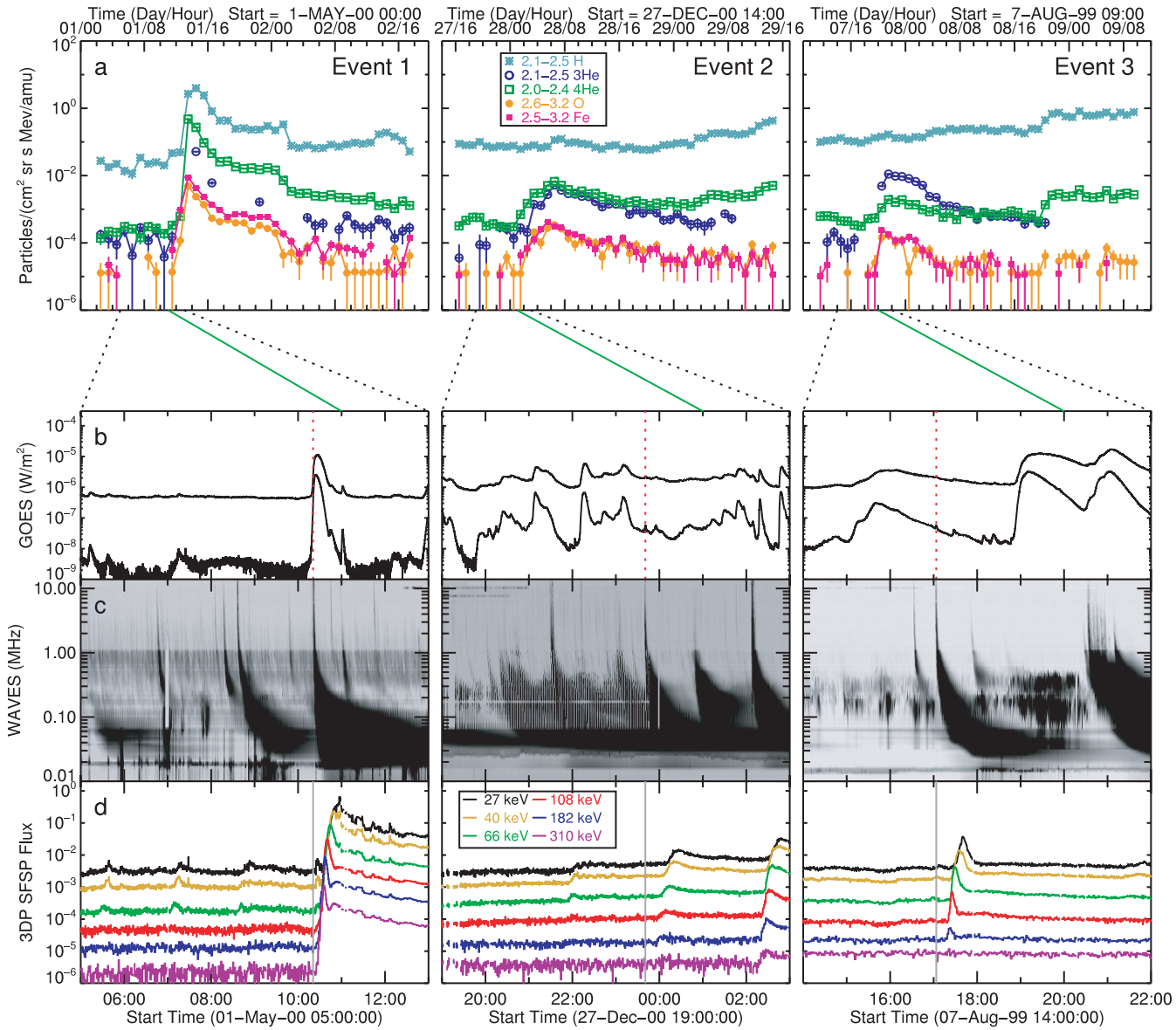

FIG. 1.—Three examples of impulsive SEP events. Ion time profiles from LEMT are shown in panel *a*. The other panels show (*b*) *GOES* X-ray (1–8 Å and 0.5–4 Å) fluxes, (*c*) *Wind* WAVES radio spectra, and (*d*) *Wind* 3DP electron fluxes for the time intervals around the ion onset as marked by the green lines. The time of the type III burst and hence the assumed ion injection is indicated by the dotted red line and solid gray line in the panels *b* and *d*, respectively. The dotted lines between the panels *a* and *b* show the time ranges of the bottom panels with respect to the ion time profiles.

burst in event 4 is very weak above 1 MHz. For event 5, we find multiple type III bursts, but none of them are intense. Here we choose the one shortly after 06 : 00 UT because of its visibility at 10 MHz and a clearer extension to low frequencies than another at 04 : 45 UT. Similar considerations apply to event 6.

We immediately note that, except for event 1, the type III bursts are not correlated with major flares in the *GOES* 1–8 Å light curves. Small increases in the *GOES* light curves could occur while larger flares are still ongoing (e.g., event 3), and they can be at different locations. These small brightenings are usually not included in the Hα flare list maintained by the National Geographical Data Center.[6] Therefore we need to examine full-disk images to locate the source region as brightenings associated with the type III bursts.

[6] See http://www.ngdc.noaa.gov/stp/SOLAR/ftpsolarflares.html.

2.2. *Identification of Solar Sources in EUV/X-Ray Images*

Our search of brightenings is based primarily on EIT images, but we also use SXT images when available. EIT usually takes full-disk images at a ~12 minute regular cadence. For most times, these images are in the 195 Å channel, which is sensitive primarily to ~1.5 MK (Fe XII) plasma and secondarily to ~20 MK (Fe XXIV) plasma. SXT is sensitive to a broad temperature range above ~2 MK. Although the cadence of SXT data was irregular, with long data gaps due to satellite night as well as flare mode and data recorder overwriting, successive full-disk images could be only 2 minutes apart. It is easier to locate minor flares in SXT images, because increase in emission measure in flares is usually more pronounced at higher temperatures than at <2 MK.

Solar images for events 1–3 (Fig. 1) and events 4–6 (Fig. 2) are presented in Figures 3 and 4, respectively. For events 1–4,

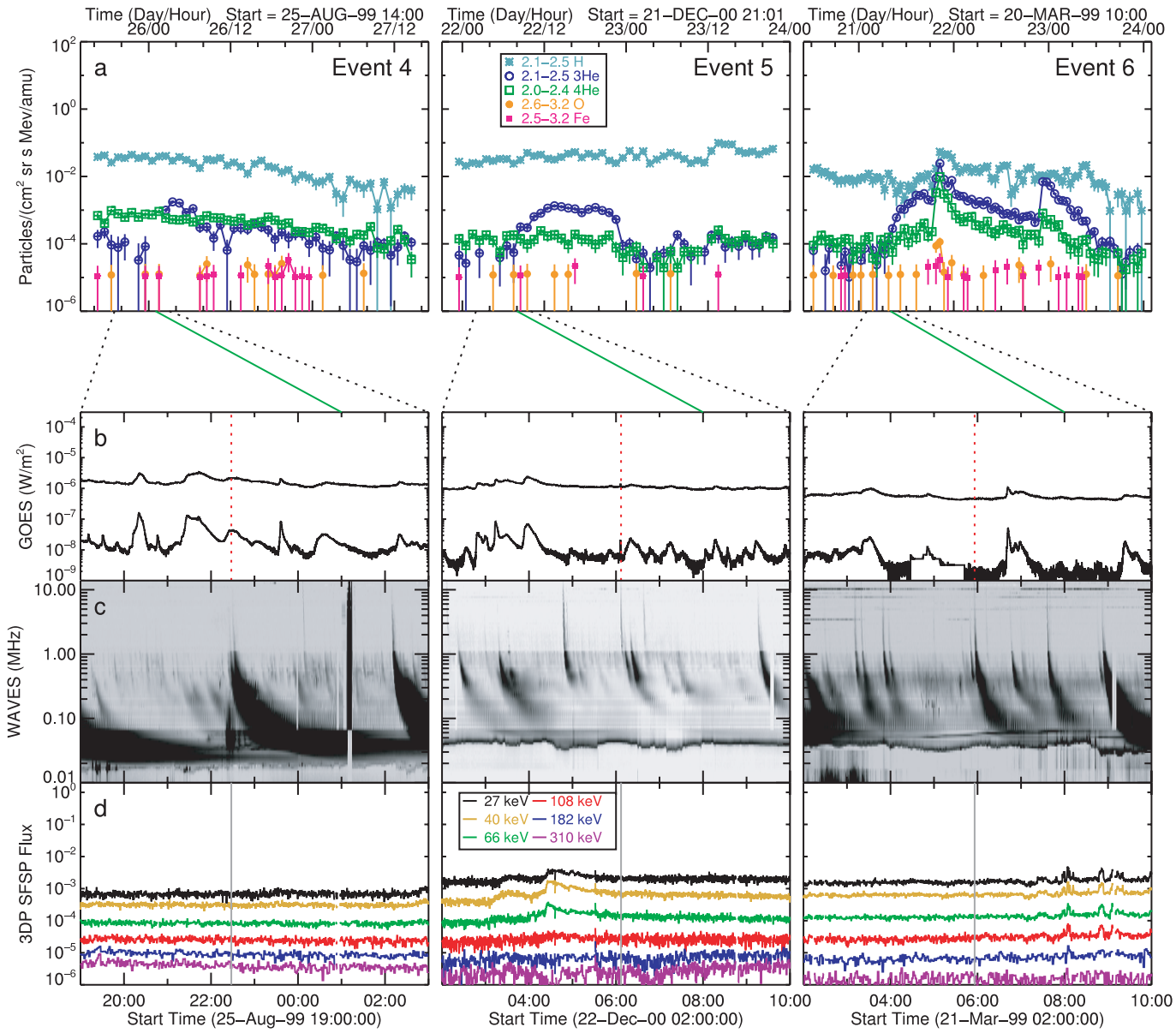

FIG. 2.—Another set of impulsive SEP events in the same format as Fig. 1. Solar sources of these events are difficult to find, because the type III bursts are weak (especially above ~1 MHz), no associated electron events are observed, or solar images do not show signatures of impulsive flares or brightenings.

the location of the brightening is outlined on the EIT images taken closest in time to the type III bursts (see Figs 3*a*–3*c*, and 4*a*). The outlined areas are enlarged in the bottom panels, where images from other instruments are shown. In Figure 3d we show hard and soft X-ray images of the M1 solar flare[7] associated with event 1. The hard X-ray image obtained by the Hard X-ray Telescope (HXT; Kosugi et al. 1991) on *Yohkoh* shows double sources, which are often interpreted as the footpoints of the flaring loop. However, HXT images in time sequence (not presented here) show that the southern source is not stationary, likely indicating changes in magnetic field topology during the impulsive phase. In events 2–4, images from the *Transition Region and Coronal Explorer* (*TRACE*; Handy et al. 1999) reveal jets shortly after the onsets of the type III bursts, which were not unambiguously seen in EIT due to its lower cadence.

In event 5, the selection of the type III burst was not straightforward. The one we selected corresponds to a localized brightening east of the central meridian, as seen in a timely SXT full-disk image (Fig. 4*e*). If we select earlier type III bursts at 02:10 UT and 03:15 UT, which do not appear to start from >1 MHz, it is not possible to find unambiguous signatures of this event in the low corona. Event 6 is even more problematic. There were no distinguishable signatures on disk around the times of type III bursts. We note, however, repeated large-scale activity over the west limb, connecting the north and south hemispheres, around the times of a certain type III bursts including the one we chose. Because of a low confidence level, we exclude this and similar events from the discussion in the next section.

3. SOLAR SOURCES

Using brightenings associated with type III bursts, we identified the solar sources of 69 impulsive SEP events in coronal

[7] A M1 flare has the peak flux I_{peak} of 1×10^{-5} W m^{-2} in the 1–8 Å channel of the *GOES* X-Ray Spectrometer. We follow the commonly used flare classes of A, B, C, M, and X, corresponding, respectively, to $I_{peak} < 10^{-7}$, $10^{-7} \leq I_{peak} < 10^{-6}$, $10^{-6} \leq I_{peak} < 10^{-5}$, $10^{-5} \leq I_{peak} < 10^{-4}$, and $I_{peak} \geq 10^{-4}$, all in the units of W m^{-2}.

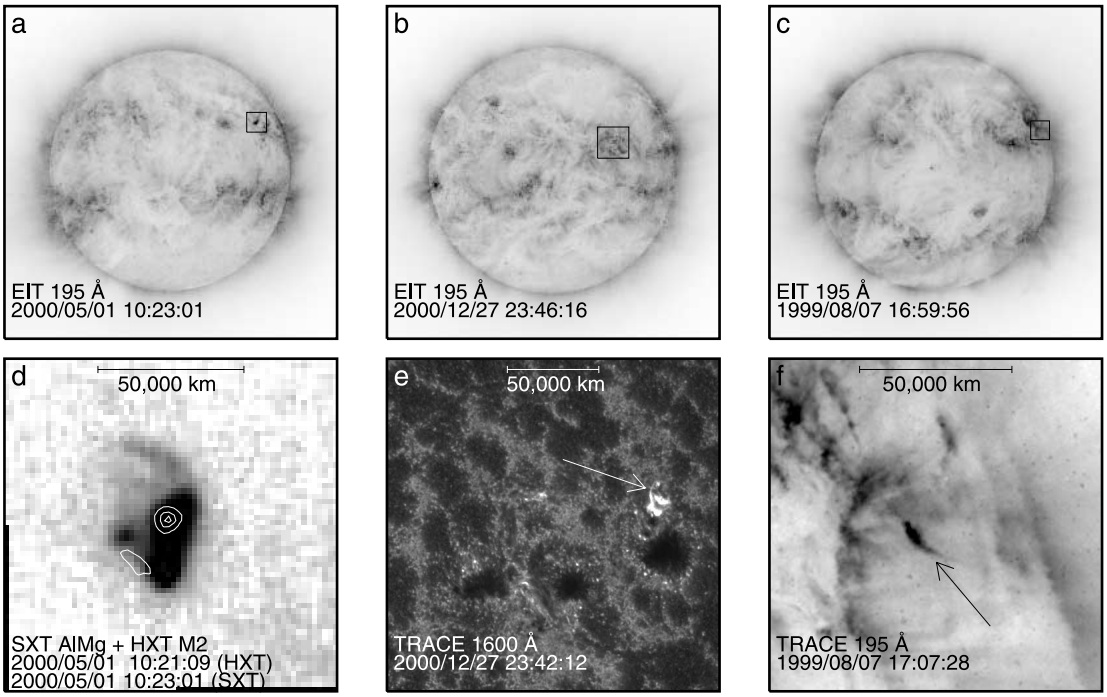

FIG. 3.—Solar images around the times of the type III bursts that we associate with acceleration of the three impulsive SEPs as shown in Fig. 1. Panels *a–c* are EIT 195 Å images for the three events on which we locate changes associated with the type III bursts. The square boxes indicate the areas in which such changes are identified. Bottom panels give enlarged views of these areas: (*d*) SXT image of a M1 flare superposed with an HXT 33–53 keV image as a contour map; (*e*) *TRACE* 1600 image showing footpoints of a jet as indicated by an arrow; (*f*) *TRACE* 195 Å image showing a jet as indicated by an arrow.

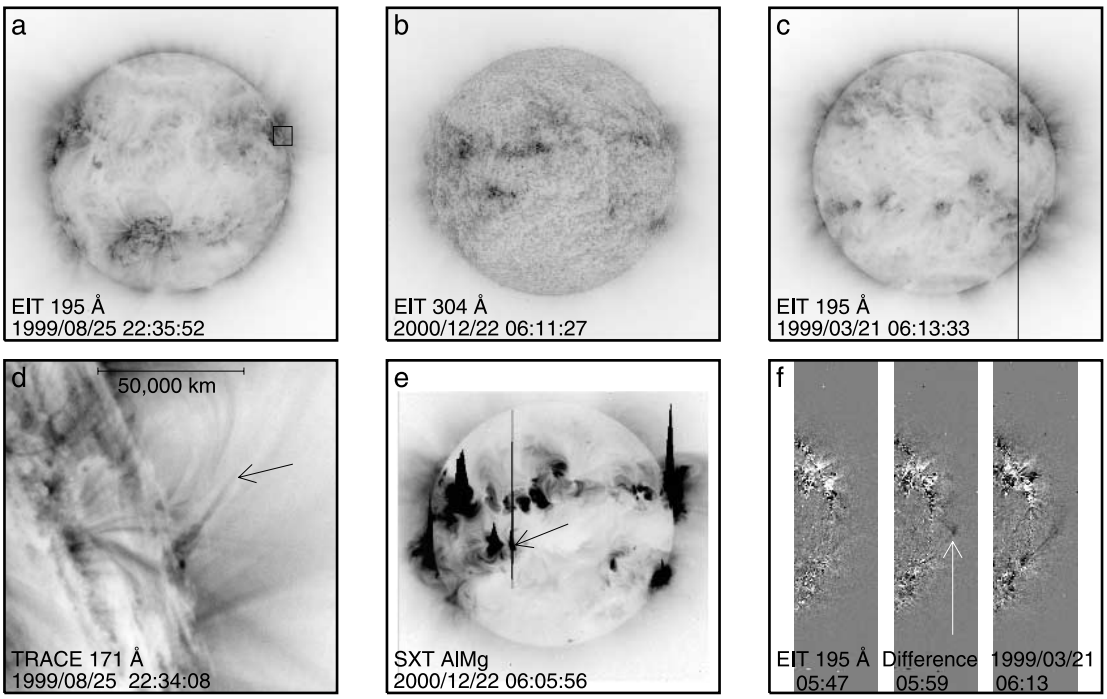

FIG. 4.— Solar images for the impulsive SEP events shown in Fig. 2. As in Fig. 3, panels *a–c* give full disk images from EIT around the times of the type III bursts. For event 4, *TRACE* 171 Å images show (*d*) a jet. The type III burst associated with event 5 corresponds to a compact brightening as found in (*e*) an SXT full-disk image. The vertical spike comes from bleeding from saturated pixels. Panel *f* gives three EIT running difference images of the west limb (as marked in panel *c*), indicating a weak transequatorial eruption.

TABLE 2

List of Impulsive SEP Events with Identified Solar Sources

SEP				CME				PFSS[b]		
								Model		
Onset Date and Time	Category	Type III Time	Flare Class	Speed (km s^{-1})	Width (deg)	Source Location	*TRACE*[c]	2.5 $R_\odot$	2.0 $R_\odot$	WSO (2.5 $R_\odot$)
1995 Mar 29 07:00	3	06:44	C1.6	NA	NA	S17 E03	...	...	...	...
1995 Apr 2 14:00	3	11:07	B2.3	NA	NA	S17 W56	...	...	...	...
1997 Sep 17 20:00	1	17:28	B9.7	613	46	S23 W70	...	1	1	...
1997 Sep 18 03:00	3	00:00	B9.7	...	...	S25 W76	...	1	1	4
1997 Sep 18 23:00	3	19:52	C1.5	343	44	S23 W90	...	3	3	4
1997 Nov 24 13:00[a]	1	12:48	B2.8	570	29	N23 W65	...	1	1	...
1998 May 17 08:00	1	04:44	B2.3	...	...	S25 W02	...	3	3	3
1998 Aug 13 15:00	1	09:28	B1.8	NA	NA	N19 E05	J (171 Å)	...	...	3
1998 Aug 15 03:00	3	00:29	C2.9	NA	NA	S25 W85	...	...	...	4
1998 Sep 27 11:00	3	08:08	C2.2	NA	NA	N21 W48	...	...	...	...
1998 Sep 28 03:00	3	23:38	C5.6	NA	NA	N20 W58	...	...	...	...
1998 Sep 29 07:00	3	01:57	C6.0	NA	NA	N23 W69	...	...	...	...
1999 Feb 20 06:00	2	04:00	C8.2	NA	NA	S18 W63	...	...	...	...
1999 Feb 20 17:00	2	15:12	C3.6	NA	NA	S21 W72	...	...	...	...
1999 Feb 21 13:00	2	09:42	C8.1	350	65	S17 W85	...	...	...	...
1999 Mar 11 02:00	2	00:06	C8.6	319	34	S18 W64	J (171 Å)	...	...	1
1999May 12 08:00	3	06:54	B2.3	224	46	S20 W90	...	1	1	1
1999 Jun 18 15:00	3	11:29	B3.3	NA	NA	N25 W90	...	4	4	3
1999 Jul 20 00:00	3	21:17	B4.9	457	17	S12 W65	...	2	2	2
1999 Jul 20 13:00	3	08:18	C1.3	...	...	S12 W72	...	1	1	1
1999 Aug 7 20:00[a]	3	17:04	B1.7	577	7	N22 W74	J (195 Å)	1	1	...
1999 Aug 26 01:00	1	22:28	B4.8	624	5	N18 W90	J (171 Å)	1	2	2
1999 Dec 26 20:00	3	16:11	B8.3	339	62	N24 W31	...	3	3	3
1999 Dec 27 07:00	2	01:48	M1.0	753	96	N24 W35	...	3	3	2
2000 Mar 7 11:00	2	07:23	C1.2	256	102	S15 W68	B (195 Å)	1	1	...
2000 Mar 7 15:00[a]	2	12:28	C1.4	391	26	S15 W72	...	1	1	...
2000 Mar 8 03:00	2	23:39	C3.5	510	13	S15 W76	PJ (195 Å)	2	1	...
2000Mar 18 23:00	2	20:52	M2.1	492	165	S14 W65	B (195 Å)	2	2	...
2000 Mar 19 15:30	2	12:44	B4.6	...	...	S18 W74	J (195 Å)	2	2	...
2000 Apr 23 04:00	3	01:15	C4.0	635	60	N16 W47	...	1	1	1
2000 Arp 24 22:00	3	19:58	C1.5	...	...	N15 W70	...	1	1	1
2000 May 1 11:00[a]	3	10:21	M1.1	1360	54	N21 W50	...	1	1	1
2000 May 4 14:00	2	11:00	C7.3	1404	>170	S17 W90	...	4	4	4
2000 May 24 01:00	3	20:48	C7.3	475	62	N21 W42	E (171 Å)	2	2	...
2000 Jun 4 09:00[a]	2	07:02	B2.0	597	17	S10 W62	...	1	1	1
2000 Aug 12 14:00	3	12:30	B5.7	434	68	N05 W48	J (171 Å)	1	1	4
2000 Aug 20 22:00	1	20:39	B2.1	...	...	N25 W60	J (171 Å)	3	3	2
2000 Aug 22 03:00[a]	2	00:07	C2.1	959	107	N30 W75	...	2	3	1
2000 Aug 22 19:00	3	18:11	C2.4	819	64	N30 W85	E (171 Å)	3	3	1
2000 Aug 23 00:00	3	21:51	B5.2	288	72	N16 W46	...	2	2	1
2000 Sep 2 12:00	1	09:40	A5.2	...	...	N12 E05	B (171 Å)	2	2	...
2000 Sep 2 22:00	1	15:40	A6.5	...	...	N12 E04	B (171 Å)	2	2	...
2000 Sep 27 08:00[a]	3	01:15	C3.5	...	...	N17 W56	B (171 Å)	1	2	1
2000 Oct 3 13:00	2	07:40	B4.5	...	...	N27 W62	...	2	2	4
2000 Oct 29 08:00	3	01:56	M4.4	NA	NA	S22 E35	...	3	3	...
2000 Dec 19 07:00	3	03:25	B9.9	598	20	N10 W66	...	1	1	2
2000 Dec 22 08:00	1	06:06	B2.5	...	...	S12 E18	...	3	3	...
2000 Dec 28 01:00[a]	3	23:40	B3.4	...	...	N13 W36	J (1600 Å)	1	1	...
2001 Feb 24 06:00	1	03:13	B1.0	...	...	S27 W26	...	4	4	...
2001 Apr 14 18:00	3	17:10	C3.9	830	113	S18 W71	E (171 Å)	3	3	...
2001 Sep 8 12:00	3	07:03	C1.5	...	...	S15 W21	...	4	4	3
2001 Sep 10 17:00	2	13:22	B6.0	293	99	N18 W90	J (171 Å)	1	1	1
2001 Sep 11 14:00	2	09:35	C8.3	294	61	N27 W90	...	2	2	4
2001 Sep 22 10:00	3	05:42	C3.2	416	74	S09 W65	...	4	3	4
2002 Feb 25 16:00	3	12:07	C1.2	...	...	S05 W51	...	4	4	4
2002 Feb 26 20:00	3	17:03	A8.3	...	...	S05 W67	PJ (195 Å)	4	4	4
2002 Apr 14 14:00	3	07:28	C1.3	757	76	N20 W66	...	1	1	1
2002 Apr 15 00:00	3	22:25	C5.4	294	27	N18 W75	...	1	1	1
2002 Apr 5 05:00	3	02:45	C7.4	674	55	N20 W79	...	1	1	1
2002 Aug 3 23:00	2	19:05	X1.0	1150	138	S16 W80	PJ (171 Å)	1	2	2
2002 Aug 4 16:00	2	14:52	C3.6	663	71	S13 W90	PJ (171 Å)	2	3	3
2002 Aug 18 23:00	2	21:10	M2.2	682	140	S13 W20	J (195 Å)	4	2	1

TABLE 2—*Continued*

SEP				CME				PFSS[b]		
								Model		
Onset Date and Time	Category	Type III Time	Flare Class	Speed (km s^{-1})	Width (deg)	Source Location	*TRACE*[c]	2.5 $R_\odot$	2.0 $R_\odot$	WSO (2.5 $R_\odot$)
2002 Aug 19 11:00[a]	2	10:30	M2.1	549	102	S12 W26	J (195 Å)	4	4	1
2002 Aug 19 23:00.....	2	20:57	M3.1	712	>66	S11 W32	J (195 Å)	4	1	1
2002 Aug 20 11:00.....	2	08:25	M3.4	1099	>122	S11 W38	J (195 Å)	4	1	3
2002 Sept 27 04:00	2	01:18	C4.2	1502	59	S15 W90	...	1	1	1
2002 Dec 10 12:00	1	0//5:16	B3.9	...	...	N15 W05	...	2	3	...
2002 Dec 12 03:00	1	00:40	B2.4	623	13	N16 W29	...	2	2	2
2002 Dec 12 15:00[a]	3	12:35	C4.5	723	51	N16 W36	...	2	2	2

[a] Events studied by Wang, Pick, & Mason (2006).
[b] This is an indicator of the combined offset d of the PFSS field line at the photosphere (from the source region) and at the source surface (from the Parker spiral coordinates). See text for definition. 1 if $d \leq 10^\circ$, 2 for $10^\circ < d \leq 20^\circ$, 3 for $d > 20^\circ$, and 4 if there are no open field lines within 10° of the source region.
[c] J: Jet, PJ: possible jet, B: brightening, E: eruption.

images. They are given in Table 2, which includes 10 SEP events studied by Wang et al. (2006). In eight of them we find the same source region.[8] This table retains the original selection criteria of the impulsive SEP events as categories 1–3, in which events are selected on the basis of whether enrichment is observed in ^{3}He or Fe or both (§ 2). The solar sources of the remaining 50 events (including two studied by Wang et al. [2006]) were not identified for the following reasons. In six events out of 110 with at least one type III burst (Table 1), we could not single out a type III burst because no particularly favorable features described in § 2.1 are observed and images indicate brightenings at different locations for different type III bursts. Furthermore, full-disk EIT or SXT images around the type III bursts were available only in 83 events. In 16 cases, we could not extract compelling signatures from images (e.g., Fig. 4*f*).

In Figure 5 we show the distribution of the heliographic longitude for each of the three categories of impulsive SEP events. We note more events enriched in ^{3}He (categories 1 and 3) from longitudes that are usually not thought of as well connected. Another difference between ^{3}He-rich and Fe-rich events is seen in the intensity distribution of the associated flares (Fig. 6). In short, more intense flares tend to be associated with category 2 (enriched in Fe but not in ^{3}He) impulsive SEP events, a tendency enhanced by excluding limb events, which can be partially occulted. Note that the soft X-ray flux reflects background subtraction which is essential for small flares as presented in Figures 1 and 2. Having indicated possible differences for impulsive SEP events selected from different criteria, however, we caution that the different categories of impulsive SEP events may arise due to the limited sensitivity of the LEMT instrument and that their distinction may not be physical.

We studied LASCO data to search for CMEs associated with impulsive SEP events with a criterion that their estimated onset times are within an hour from the type III bursts. For the entire sample, a total of 75 type III bursts occurred during LASCO data coverage, and about 60% (46) of the events have an associated CME (Table 1). This ratio is somewhat higher (39/58 or ~67%) for the events with the source location identified (Table 2), even if we impose the additional requirement that the central position angle of the CME be in the same quadrant as the source region. The true CME association could be even higher, because LASCO does not have infinite sensitivity and may miss small CMEs from disk regions (see Yashiro et al. 2005). The CMEs associated with our impulsive SEP events have varied speeds and widths, consistent with an earlier study by Yashiro et al. (2004) for a smaller sample. It is true that many of them are narrow as in Kahler et al. (2001), but wide CMEs are also associated (see Gopalswamy et al. 2003); a total of nine associated CMEs are wider than 100°. Nevertheless, none of them qualify as full halo CMEs that often accompany large gradual SEP events. We also find little evidence in WAVES data for CME shocks that appear as DH type II bursts, with a possible exception of the event on 2000 May 4. Lastly, only five events in Table 2 are clearly associated with metric type II bursts, consistent with an earlier study by Yashiro et al. (2004), which provides another argument that particles in impulsive SEP events are not produced by coronal shocks.

[8] The times of the type III bursts in the 2000 September 27 and December 28 events are a few hours earlier than the EIT event times given by Wang et al. (2006), but the source locations are consistent in the two studies. In both cases, we observed repeated brightenings in the same region.

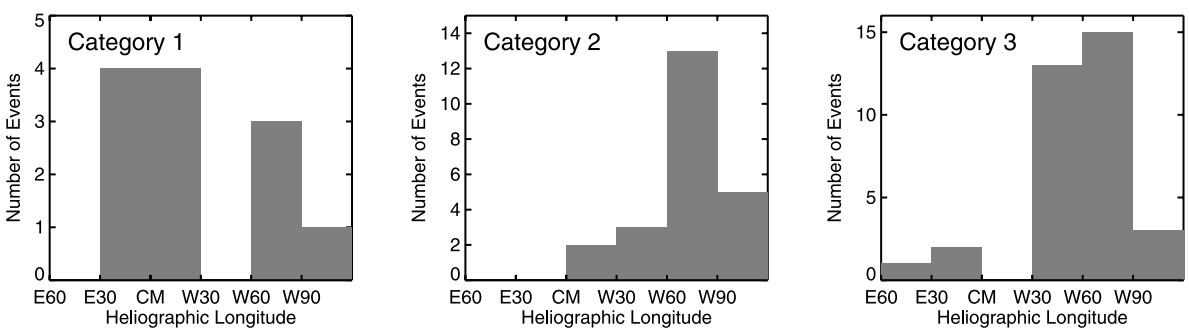

Fig. 5.—Longitude distributions of the source regions of the impulsive SEP events, as plotted separately for different ion properties.

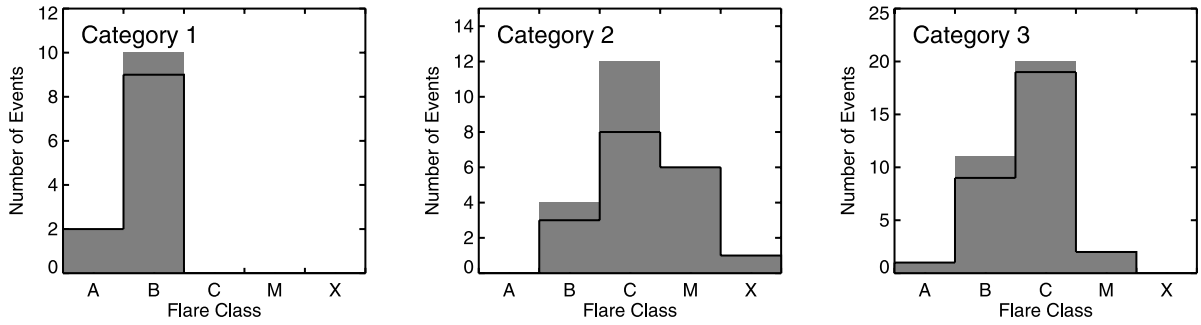

FIG. 6.—Peak intensity of the flares or brightenings associated with the type III bursts and impulsive SEP events. Solid lines exclude limb events, which may be partly occulted.

In addition to brightenings, what are the characteristic signatures of the type III bursts that may be linked with impulsive SEP events? According to Wang et al. (2006), 13 of the 25 impulsive SEP events they studied are associated with jets in EIT images. In this study, we looked for jets in data from *TRACE*, whose much higher cadence than EIT facilitates unambiguous detection of jets as narrow moving structures. The limited field of view limits the number of the source regions observed by *TRACE* to 25. A jet is identified shortly after the type III burst in 13 cases. Including possible jets, the number increases to 17. In the remaining eight events, *TRACE* images show either flare loops or motions that look like filament eruptions. Indeed, all of the latter cases are associated with CMEs.

4. MAGNETIC FIELD CONNECTION

If particles in impulsive SEP events are accelerated in impulsive solar flares, which tend to be compact, the magnetic field connection between the flare region and the Earth determines whether such particles are detected at 1 AU. In this section, we evaluate the accuracy of a technique that reveals where on the Sun the Earth-intersecting magnetic field comes from, using the locations of the source regions of impulsive SEP events as given in the previous section. The technique combines the Parker spiral for the interplanetary magnetic field with the potential field source surface (PFSS) model (Schatten et al. 1969) for the coronal magnetic field. It is widely used in heliophysics research (e.g., Neugebauer et al. 2002), where its performance is often measured in terms coronal hole boundaries in the corona and solar wind speeds observed typically at 1 AU. Our study of impulsive SEP events gives an independent metric.

Our evaluation of the technique is based on how often it indicates magnetic connectivity to within some given distance of the SEP source region. The result is given in § 4.3.

4.1. *The Technique*

Here we give a summary of the technique. First, the division between the coronal and interplanetary regimes is located at the source surface at 2.5 $R_\odot$ from Sun center, a set radius that approximates the transition from low to high plasma β. In the coronal volume between the photosphere and the source surface, the magnetic field is assumed to be potential (i.e., current-free). Those photospheric fields that reach the source surface are called open, where they are forced to be radial. Exterior to the source surface, the magnetic field lines take the shape of the Parker spiral in the interplanetary space as a result of the radial solar wind (assumed to have a constant speed) and solar rotation.

In the PFSS model, the lower boundary condition comes from synoptic magnetograms taken somewhere near the base of the corona, typically the photosphere. In our definition, "synoptic" maps of the photospheric magnetic field are unavailable, in the sense of "instantaneous" data for the full sphere of the Sun. Not only is the non-Earth-facing side of the Sun unobserved, but also polar regions and regions close to the limb are poorly observed by current array of full-disk magnetographs. We choose to base the PFSS extrapolation on synoptic magnetic maps that are calculated with the evolving surface flux model of Schrijver (2001). In this model, magnetic flux is continually transported horizontally across the model photosphere by differential rotation, poleward meridional flows, and stochastic diffusion processes. When available, full-disk magnetograms from the Michelson Doppler Imager (MDI; Scherrer 1995) are directly inserted into the model. After this insertion process, the evolutionary mechanisms take over and continue to evolve these flux patterns even as their longitudes of insertion rotate out of view. In contrast, the evolution of flux contained in traditional synoptic maps is frozen once this flux is not positioned on the Earth-facing side of the Sun. Such evolving maps are sampled every six hours. Our standard synoptic map has equal-area pixels with the resolution of 1 deg^2 at the equator. See Schrijver & DeRosa (2003) for a full description of the procedure.

In order to see if the source regions of impulsive SEP events are well connected, we trace field lines back from 1 AU through the Parker spiral, and back through the corona to the photospheric source regions as determined by the PFSS model, using the synoptic maps that are closest in time to the type III bursts. We study a subset of 58 events from Table 2. The remaining 11 events were either unobserved by MDI or too soon after long data gaps for the flux dispersal model to work properly.

4.2. *Open Flux*

Before tracing field lines, we study the magnetic field connectivity within the corona, and find whether the SEP source regions contain open field. In Figure 7, we show open field lines overplotted on the EIT images that are given in Figures 1 and 2. We correct for solar rotation between the EIT image and the synoptic magnetogram. These field lines are traced from a uniformly spaced grid on the source surface back to the photosphere. They are shown in green and pink for their positive and negative polarities, respectively, at the photosphere. Yellow lines stand for special field lines whose latitudes at the source surface correspond to the ecliptic plane. They can potentially intersect the Earth, assuming no latitudinal excursion between the source surface and 1 AU. For each of events 1–5, the identified source region is indicated as a blue circle (Figs. 7*a*–7*e*). For event 6, we could not convincingly identify the source region, apart from eruptive signatures over the west limb, but their relation to open field is

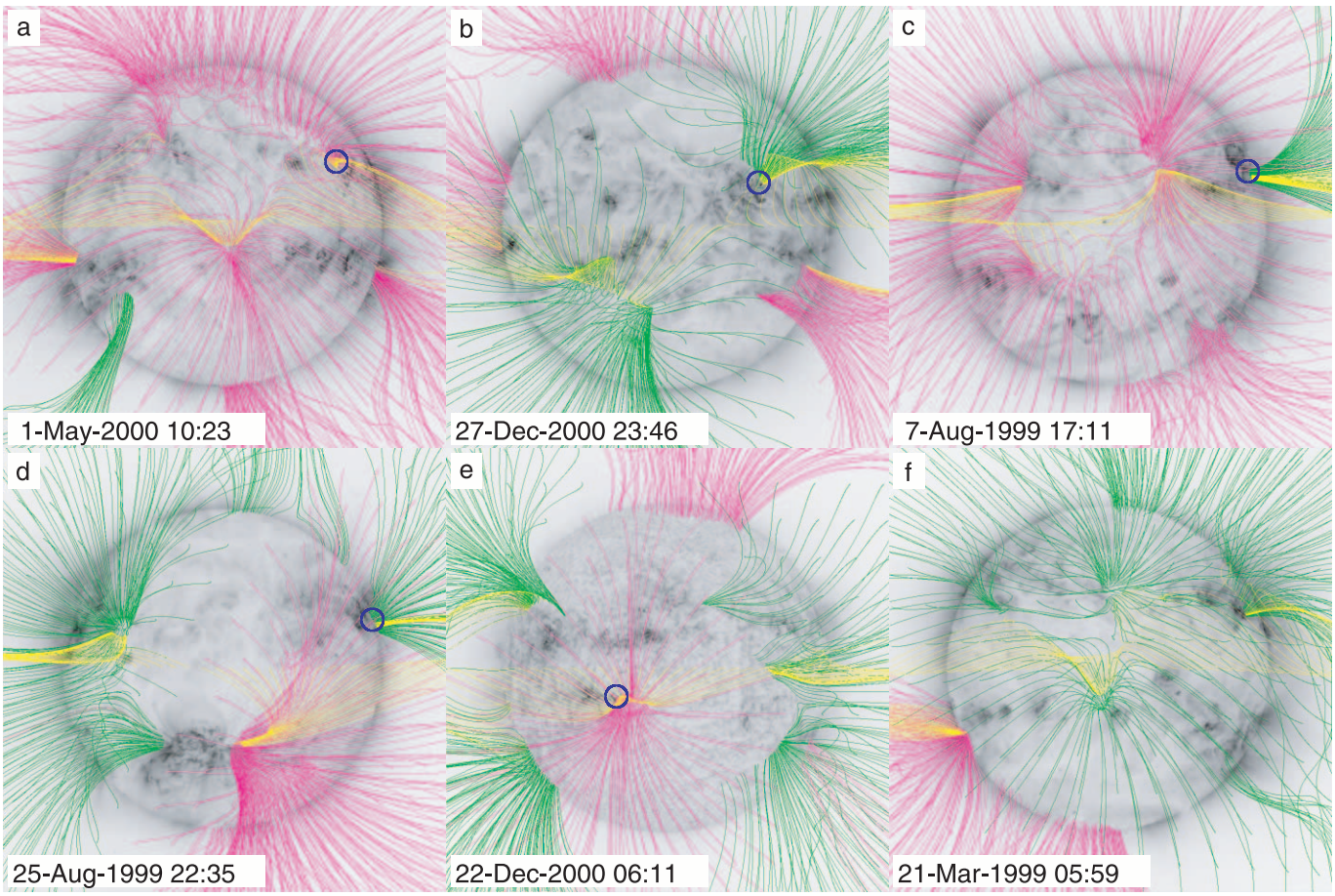

FIG. 7.—Open field lines as plotted on the EIT full-disk images that are shown in Figs. 2 and 4. These field lines are calculated with the PFSS model on the flux dispersal model assimilated into MDI magnetograms. Pink and green stand for negative and positive footpoint polarities, respectively. Yellow indicates the field lines that reach the source surface (at 2.5 $R_\odot$) at the ecliptic. Circles in blue show the source locations of the impulsive SEP events. Panel *f* does not include such a circle because we could not identify the source low in the corona.

not clear (see Fig. 7*f*). As shown in Figures 7*a*–7*e*, the source regions of events 1–5 have open field lines, some of which are ecliptic. In ~80% (47/58) of the cases, open field lines can be found within 10° from the source region.

4.3. *Footpoints of Field Lines Connected to the Earth*

We now determine whether the computed open field lines from the source regions are connected to the Earth. The Parker spiral field line that reaches the Earth crosses the source surface at the coordinates (ϕ_{ss}, B_0). Here B_0 is the heliographic latitude of the disk center, and the longitude ϕ_{ss} is a function of the solar wind speed. We first compare the longitude of the source region ϕ_{flare} with that of the footpoint of the field line that intersects the Earth. In Figure 8, the offset in longitude $\Delta\phi$ is plotted against the source's longitude as given in Table 2. Figure 8*a* plots the quantity $\phi_{flare} - \phi_{ss}$, assuming the straight extension of the Parker spiral (without the PFSS extrapolation) to the photosphere. In Figures 8*b* and 8*c*, we show how the PFSS model takes field

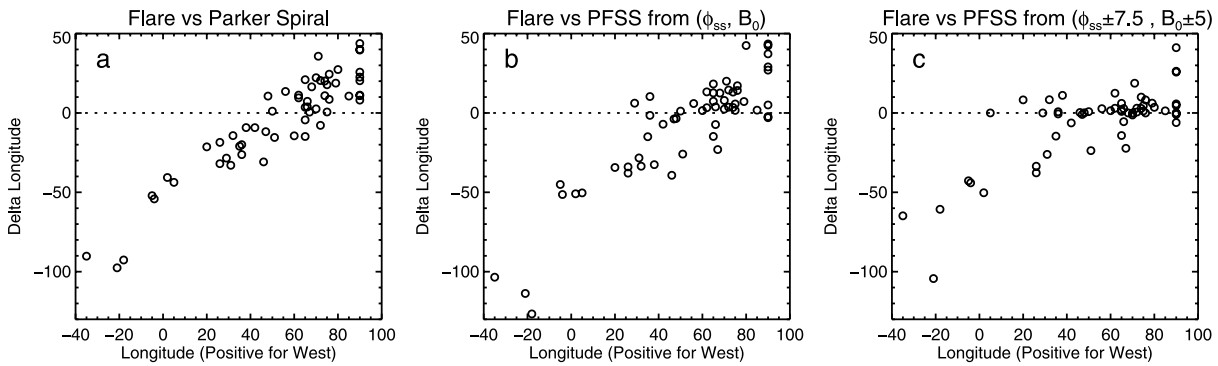

FIG. 8.—Difference in longitude between the source regions and the footpoints of the Sun-Earth field lines, plotted against the source's longitude. Straight extension of the Parker spiral to the photosphere is assumed in (*a*). In (*b*), only one PFSS field line is traced from the Parker spiral coordinates on the source surface (ϕ_{ss}, B_0). In (*c*) field lines are traced from ($\phi_{ss} \pm 7.^\circ5$, $B_0 \pm 5.^\circ0$), and the minimum difference in longitude is plotted.

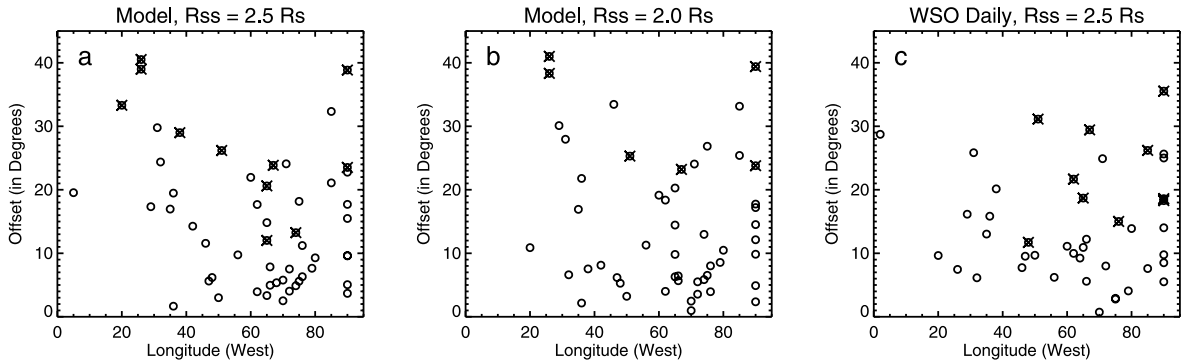

FIG. 9.—Combined offset at the photosphere and the source surface plotted against the source's longitude as given in Table 2. Crosses are overplotted when there are no open field lines within 10° of the source region. In (*a*) the standard PFSS extrapolation is performed on our MDI-assimilated synoptic maps. In (*b*) we change the source surface radius from 2.5 to 2.0 $R_\odot$. In (*c*) daily updated synoptic maps from the Wilcox Solar Observatory are used.

lines closer in longitude to the source regions. In Figure 8*b* we trace only one field line that crosses (ϕ_{ss}, B_0). We note that $\Delta\phi$ does not significantly decrease. Obviously tracing one field line is not realistic, given various uncertainties of the interplanetary magnetic field including nonconstant solar wind speed. Therefore, we trace field lines whose source surface coordinates are within ($\phi_{ss} \pm 7.^\circ5$, $B_0 \pm 5.^\circ0$), and plot the minimum difference in photospheric longitude (Fig. 8*c*). It is clear that the PFSS model makes the difference in longitude much smaller for many events. But it should also be noted that well-connected field lines are never anchored in the eastern hemisphere in the PFSS model.

In order to further evaluate the technique, we need to include the difference in latitude. Let the open field lines have heliographic coordinates (ϕ_0, θ_0) and (ϕ_1, θ_1) at the photosphere and the source surface, respectively. We search for the field line that minimizes the combined offset d at the photosphere d_p and the source surface d_{ss}, defined as $d = (d_p^2 + d_{ss}^2)^{1/2}$, where $d_p = \left[(\phi_0 - \phi_{flare})^2 + (\theta_0 - \theta_{flare})^2\right]^{1/2}$ and $d_{ss} = \left[(\phi_1 - \phi_{ss})^2 + (\theta_1 - B_0)^2\right]^{1/2}$. Here we neglect the latitudinal foreshortening because most of the field lines are confined to low latitudes.

The combined offset is plotted in Figure 9*a* against the source longitude from Table 2. We exclude the sources in the eastern hemisphere for a better view of those in the western hemisphere with smaller offsets. Here we group the results into four classes: 1 for $d \le 10^\circ$, 2 for $10^\circ < d \le 20^\circ$, 3 for $d > 20^\circ$, and 4 for the cases where no open field lines are found within 10° from the flare location. We have 23, 15, 9, and 11 class 1, 2, 3, and 4 cases, respectively (see Table 2). At face value, the PFSS and Parker spiral approximations do a reasonable job of connecting the impulsive SEP event with its source region. However, of the 23 class 1 cases, only nine have an offset less than 5°. This result, along with the fact that there are 11 cases in which no open field lines fell near the source region, leads us to conclude that the technique does not provide a realistic Sun-Earth magnetic field connection to the level. We need more accurate mappings to understand the relation of the SEP acceleration with solar flares. Such mappings may require more physically realistic coronal and heliospheric field models, which may ultimately require vector magnetic field over the full sphere. Unfortunately, they appear to be unavailable in the foreseeable future.

The results arising from such PFSS extrapolations may depend to some extent on the boundary conditions. Therefore we repeat the analysis for different settings. First, in an expectation that some tall closed structures may become open, we change the standard radius of the source surface from 2.5 to 2.0 $R_\odot$ (Fig. 9*b*). After this adjustment, five of the class 4 cases have been changed to class 1–3, although the overall results are very similar and the numbers of class 1 and 2 events stay almost the same (Table 2). Alternatively, we use daily updated synoptic maps from the Wilcox Solar Observatory (WSO), which have 5° resolution instead of 1° in the evolving flux transport model. The number of cases we study is 45, because we do not use data from periods of poor observing conditions. The offset is plotted in Figure 9*c*. The breakdown of the classes is 19, 8, 8, and 10 for classes 1, 2, 3, and 4, respectively (Table 2). Although the distribution in these classes is more or less similar in the three PFSS settings, different regions are marked as "no open field." Therefore we confirm that the magnetic connectivity of the source regions of impulsive SEP events somewhat depends on how the PFSS extrapolations are made, yet it is not clear whether certain settings are better than any of the others.

5. DISCUSSION

We have studied the solar sources of impulsive SEP events using coronal images. This task is not straightforward mainly for the following reasons. First, it is difficult to determine the injection time from the time profiles of low energy (~2 MeV amu^{-1}) ions alone. Even if one can perform the velocity dispersion analysis, first-arriving particles may not be scatter-free (see Lintunen & Vainio 2004). In this work, we use type III bursts observed by WAVES so that we limit the times of possible changes in the corona that may have to do with ion acceleration. But we encounter another difficulty of selecting the right type III burst especially in the absence of an electron event. Second, once the type III burst is selected, we cannot always locate it, partly because full-disk images are not available during the associated short-lived brightening. More importantly, a tiny brightening does not always produce signals in EUV images distinguishable from other ongoing activities in the corona. Despite these constraints, we are able to locate the solar source of about 60% of the impulsive SEP events selected from LEMT data, using rather extreme criteria on abundances (^{3}He/^{4}He > 0.5 or Fe/O > 0.5).

Consistent with previous results, the solar sources of impulsive SEP events tend to be weak in terms of the X-ray flux; identification of the source regions would be erroneous without using images. Enrichment in ^{3}He (Reames et al. 1988) and heavy ions (Reames & Ng 2004) has been shown to be anticorrelated with the peak X-ray flux of the associated flares. We find some major flares associated with impulsive SEP events, but all of them are Fe-rich (Fig. 6). In contrast, the solar sources of impulsive SEP events enriched only in ^{3}He (category 1) correspond to brightenings below the *GOES* C-level, and they are more often located in longitudes generally thought of as

poorly connected than Fe-rich events (categories 2 and 3; see Fig. 5). These observations may at first sight appear to support the ad hoc scenario proposed by Cliver & Kahler (1991) in which Fe ions are accelerated in flares low in the corona, whereas ^{3}He ions are accelerated in high coronal flares (at the altitudes of $>0.5\ R_\odot$), similar to the impulsive 2–10 keV electron events lacking spectral hardening toward low energies which would be caused by Coulomb collisions (Potter et al. 1980).

The paper by Cliver & Kahler (1991) uses the fact that ^{3}He/^{4}He and Fe/O are uncorrelated (e.g., Mason et al. 1986) to suggest that ^{3}He and ^{4}He are accelerated at a different altitude from Fe and O. Unfortunately, it is also true that abundance ratios, such as ^{4}He/H, ^{4}He/C, ^{3}He/^{4}He, and Fe/C are all uncorrelated with each other (Reames 2000). In addition, abundances of other species, such as N, Ne, Mg, and Si, are also uncorrelated (Reames 2000). Recently, it has been found that $(33 < Z < 40)$/O, $(49 < Z < 56)$/O, and $(78 < Z < 82)$/O are all uncorrelated with Fe/O and with ^{3}He/^{4}He in impulsive events (Reames & Ng 2004). Like those for ^{3}He, the heavy-element enhancements also decrease with event size. It is extremely difficult to believe the lack of correlation to imply that each element and isotope is accelerated at a different solar altitude, especially since all elements arrive at 1 AU with essentially the same onset time. While the element correlations are not understood quantitatively, it is easier to believe that a complex spectrum of resonant waves, in the flare site, varies from event to event, producing abundance variations that seem random to us.

We believe that a simpler explanation of the differences of event size for the three event categories lies essentially in instrument bias, i.e., small ^{3}He-rich events are simply easier to see than small Fe-rich events. Because He/O $\gg 1$ in the corona, we can easily measure ^{3}He/^{4}He in small SEP events where Fe and O intensities are well below instrument threshold. This may explain the existence of category 1 events, whose solar sources tend to be smaller flares than those of category 2 and 3 events. Furthermore, it is known that the ^{3}He/^{4}He ratio decreases with increasing flare energy (Reames et al. 1988). This may result from ^{3}He ions being depleted with increasing energy input (Reames 1999). The existence of category 2 events, associated with larger solar flares, may be explained in terms of the difficulty of measuring a small ^{3}He/^{4}He with LEMT.

While we study the solar sources of impulsive SEP events more closely using *TRACE* data, we often, but not always, observe a jet 2–5 minutes after the onset of the type III burst. As shown by Shimojo & Shibata (2000), the jets can be understood in terms of the interaction of emerging flux with preexisting open field. To determine whether the observed jets do represent plasma motions along open field lines rather than in very tall but closed structures, the temporal association with type III bursts is a key. It is also helpful to identify them in coronagraph data (Wang & Sheeley 2002), but distinguishing jets from CMEs in the usual sense (i.e., ejections adding new magnetic flux to the interplanetary space) may not be trivial from coronagraph data alone. In fact, Wang et al. (2006) listed the white-light counterparts of some of the EUV jets as CMEs. The general lack of type II bursts indicates that impulsive SEPs are not shock-accelerated even if CMEs are observed, and that these CMEs are at least qualitatively different from more extended ones often accompanying gradual SEP events.

EUV and X-ray images do not allow us to unambiguously locate small open field regions that are characteristic of impulsive SEP regions. We also point out that He I λ10830 images often fail to reveal these regions as in the case for narrow coronal holes (Arge et al. 2003). We need to rely on magnetic field models, and the PFSS model is the only operational model that can handle large-scale magnetic field.

The PFSS model shows that $\sim$80% of the source regions we identify have open field lines within 10° from the flare locations, and that in $\sim$40% ($\sim$15%) is the combined offset at the photosphere and the source surface (as defined in § 4.2) less than 10° (5°). These numbers suggest the potential usefulness of the technique (as in other applications), but they also indicate that the technique is not accurate enough for locating the solar sources of impulsive SEP events when imaging data do not help. Of course, we cannot say for sure that the identification of the source regions is completely correct, but in most of the events included in Table 2, there is little ambiguity of either the type III burst or its associated brightening in the corona. The large offset may partly come from our simplified assumption of the constant solar wind speed that results in interplanetary magnetic field described as the simple Parker spiral. But here we consider the possible limitations of the PFSS model for the coronal magnetic field.

First, the magnetic field connection between the photosphere and the source surface does not appear to be as simple as that given by the PFSS model. The repeated dropouts of the particle flux in some impulsive SEP events with a timescale of $\sim$3 hr (Mazur et al. 2000) indicate complex magnetic field connection, possibly supporting the random walk magnetic field mixing (e.g., Jokipii & Parker 1969). The lack of such complexities in the PFSS model may partly reflect the limited resolution of the standard photospheric magnetograms (1°–5°), which may smear out compact open field regions, but we report that increasing the resolution to $0.^\circ5$ essentially does not change the connectivity between the photosphere and the source surface.

Second, validation of the PFSS model usually involves limited observations, such as the coronal hole boundaries seen in images and solar wind speeds measured typically at 1 AU. Concerning solar observations, apart from large coronal holes, it is often unclear, a priori, which parts of the Sun, as imaged at certain wavelengths, contain magnetic field that is open to the interplanetary space. The areas that contain open magnetic field may incessantly change as a result of reconnection between open and closed field lines (Fisk 2005). Furthermore, apparent matches of the PFSS field lines with observed active region loops (e.g., Schrijver et al. 2005) still need more quantifiable criteria. It is also possible that the solar wind speed, on the basis of the expansion of magnetic field at the source surface, may not serve as a good test for the model, except for large coronal holes for fast wind; slow wind could arise from almost anywhere with stronger photospheric fields. Lastly, we point out that the three-dimensional structure of the streamer belt is another example in which the PFSS model gives a structure that is roughly consistent with the observations, but it fails to reproduce smaller structures in the data (Saez et al. 2005).

One more factor that needs to be addressed when discussing extrapolations of the global solar magnetic field is the possible effect of unobserved and poorly observed areas of the Sun. Newly emergent flux in those areas is hardly accounted for, even though the synoptic maps we use reflect the evolution of the surface field as calculated with the flux dispersal model (Schrijver 2001; Schrijver & DeRosa 2003). Since the source regions of our impulsive SEP events are more often in the western hemisphere, we cannot rule out the possibility that the unseen evolution of the region behind the west limb could in certain cases affect the magnetic field topology around the source region.

This lack of the simultaneous magnetogram on the full surface of the Sun will continue to pose a major challenge on our understanding of the heliospheric magnetic field.

Our results may at first sight look contradictory to Wang et al. (2006), who found Earth-directed field lines next to the source regions of their 25 ^{3}He-rich events with the average angular separation of $\sim 4^\circ$. There seem to be three reasons for the apparent differences. First, the source regions in Wang et al. (2006) were restricted to the longitude range of W20–W90. We have no such selection bias as to the longitude, and even include regions in the eastern hemisphere as long as we recognize brightenings around the times of type III bursts. The PFSS model will not map the field lines from such regions to the well-connected longitudes on the source surface. Second, the better match of the footpoints of the well-connected field lines to the source regions in Wang et al. (2006) is partly because they traced field lines from a quite large area on the source surface. Their Earth-directed field lines were defined as intersecting the source surface over the longitude range W35–W65 and over the latitude range $(B_0 - 20^\circ, B_0 + 20^\circ)$. We include only those field lines that intersect the source surface over the longitude range $(\phi_{ss} - 7.^\circ5, \phi_{ss} + 7.^\circ5)$, where ϕ_{ss} is determined by the solar wind speed, and over the latitude range $(B_0 - 5^\circ, B_0 + 5^\circ)$. Third, Wang et al. (2006) used magnetograms from the National Solar Observatory at Kitt Peak or from the Mount Wilson Observatory, whereas we use magnetic maps that come from MDI magnetograms assimilated into the evolving surface flux model. As we have seen in § 4, the PFSS extrapolated field depends to some extent on the magnetograms used as the lower boundaries.

Lastly, this study is based on impulsive events identified in narrow energy ranges with rather extreme criteria for the abundance anomalies. It has been shown that spectra of different ions over a wide range of energy reveal a variety, suggesting the presence of different acceleration mechanisms in the source (Mason et al. 2002). The solar sources may vary for impulsive SEP events at different energies and with different selection criteria.

6. SUMMARY

1. We identify the solar sources of 69 impulsive SEP events observed at 2–3 MeV amu^{-1}, using EUV and X-ray full-disk images taken around the times of the associated type III bursts. This represents about 60% of the original list of impulsive SEP events. The solar sources of the remaining events will need higher cadence full-disk images with broader temperature coverage.

2. The solar sources tend to be minor flares, although a small number of events are associated with X- and M-class flares. They are more often located in the longitudes often referred to as "well connected," but ~20% of the events are located elsewhere.

3. The CME association is higher than previously shown, but this may be due largely to the increased sensitivity of LASCO. More importantly, we seldom observe type II bursts associated with impulsive SEP events, keeping them separate from shock-accelerated gradual SEP events.

4. Consistent with Wang et al. (2006), we consider jets associated with type III bursts to be an important observable for impulsive SEP events. They represent flaring that involves open field lines.

5. The identified source regions of impulsive SEP events are used to evaluate the technique that combines the PFSS model and the Parker spiral, independent of the solar wind speed and the polarity of the interplanetary magnetic field. Our results suggest that we need a more sophisticated technique and extensive data to better understand the Sun-Earth magnetic field connection. Consequently, it is still not clear whether all the impulsive solar flares give rise to impulsive SEP events when they occur in well-connected regions, or the solar flares responsible for impulsive SEP events belong to a special class.

This work was initiated by discussions at the Living With a Star Coordinated Data Analysis Workshop (2002 July). We thank the referee for useful comments that clarified several unclear points in the original manuscript. We acknowledge the *SOHO*, *Yohkoh* and *Wind* instrument teams and the Wilcox Solar Observatory for making the data available. The efforts of N. V. N. and M. L. D. have been supported by NASA and NSF grants and Lockheed Martin funding for R&D.

REFERENCES

Arge, C. N., Harvey, K. L., Hudson, H. S., & Kahler, S. W. 2003, in AIP Conf. Proc. 679, Solar Wind 10, ed. M. Velli, R. Bruno, & F. Malara (Melville: AIP), 202
Bougeret, J. L., et al. 1995, Space Sci. Rev., 71, 231
Brueckner, G. E., et al. 1995, Sol. Phys., 162, 357
Cliver, E. W., & Kahler, S. W. 1991, ApJ, 366, L91
Delaboudinière, J.-P., et al. 1995, Sol. Phys., 162, 291
Fisk, L. A. 2005, ApJ, 626, 563
Gopalswamy, N., Yashiro, S., Kaiser, M. L., & Howard, R. A. 2003, Adv. Space Res, 32, 2613
Haggerty, D. K., & Roelof, E. C. 2002, ApJ, 579, 841
Handy, B. N., et al. 1999, Sol. Phys., 187, 229
Jokipii, J. R., & Parker, E. N. 1969, ApJ, 155, 777
Kahler, S. W., Lin, R. P., Reames, D. V., Stone, R. G., & Liggett, M. 1987, Sol. Phys., 107, 385
Kahler, S. W., Reames, D. V., & Sheeley, N. R., Jr. 2001, ApJ, 562, 558
Kahler, S. W., Reames, D. V., Sheeley, N. R., Jr., Howard, R. A., Koomen, M. J., & Michels, D. J. 1985, ApJ, 290, 742
Kahler, S. W., Sheeley, N. R., Jr., Howard, R. A., Koomen, M. J., Michels, D. J., McGuire, R. E., von Rosenvinge, T. T., & Reames, D. V. 1984, J. Geophys. Res., 89, 9683
Kahler, S. W., Sheeley, N. R., Jr., & Liggett, M. 1989, ApJ, 344, 1026
Kane, S. R. 1981, ApJ, 247, 1113
Kosugi, T., et al. 1991, Sol. Phys., 136, 17
Krucker, S., Larson, D. E., Lin, R. P., & Thompson, B. J. 1999, ApJ, 519, 864
Kundu, M. R., Raulin, J.-P., Nitta, N., Hudson, H. S., Shimojo, M., Shibata, K., & Raoult, A. 1995, ApJ, 447, L135
Lin, R. P., et al. 1995, Space Sci. Rev., 71, 125
Lintunen, J., & Vainio, R. 2004, A&A, 420, 343
Mason, G. M., Reames, D. V., Klecker, B., Hovestadt, D., & von Rosenvinge, T. T. 1986, ApJ, 303, 849
Mason, G. M., et al. 2002, ApJ, 574, 1039
Mazur, J. E., Mason, G. M., Dwyer, J. R., Giacalone, J., Jokipii, J. R., & Stone, E. C. 2000, ApJ, 532, L79
Neugebauer, M., Liewer, P. C., Smith, E. J., Skoug, R. M., & Zurbuchen, T. H. 2002, J. Geophys. Res., 107, 1488
Nitta, N. V., & Hudson, H. S. 2001, Geophys. Res. Lett., 28, 3801
Pallavacini, R. Serio, S., & Vaiana, G. S. 1977, ApJ, 216, 108
Potter, D. W., Lin, R. P., & Anderson, K. A. 1980, ApJ, 236, L97
Ragot, B. R. 1999, ApJ, 525, 524
Reames, D. V. 1999, Space Sci. Rev., 90, 413
———. 2000, in ASP Conf. Ser. 206, High-Energy Solar Physics: Anticipating HESSI, ed. R. Ramaty, & N. Mandzhavidze (San Francisco: ASP), 102
Reames, D. V., Dennis, B. R., Stone, R. G., & Lin, R. P. 1988, ApJ, 327, 998
Reames, D. V., & Ng, C. K. 2004, ApJ, 610, 510
Reames, D. V., & Stone, R. G. 1986, ApJ, 308, 902
Reames, D. V., von Rosenvinge, T. T., & Lin, R. P. 1985, ApJ, 292, 716
Saez, F., Zhukov, A. N., Lamy, P., & Llebaria, A. 2005, A&A, 442, 351
Sáiz, A., Evenson, P., Ruffalo, D., & Bieber, J. W. 2005, ApJ, 626, 1131
Schatten, K. H, & Wilcox, J. M., & Ness, N. F. 1969, Sol. Phys., 6, 442

Scherrer, P. H. 1995, Sol. Phys., 162, 129
Schrijver, C. J. 2001, ApJ, 547, 475
Schrijver, C. J., & DeRosa, M. L. 2003, Sol. Phys., 212, 165
Schrijver, C. J., DeRosa, M. L., Title, A. M., & Metcalf, T. R. 2005, ApJ, 628, 501
Shimojo, M., & Shibata, K. 2000, ApJ, 542, 1100
Tsuneta, S., et al. 1991, Sol. Phys., 136, 37
von Rosenvinge, T. T., et al. 1995, Space Sci. Rev., 71, 155
Wang, L., Lin, R. P., Krucker, S., & Mason, G. M. 2005, in Solar Wind 11, Connecting Sun and Heliosphere ed. B. Fleck, T. H. Zurbuchen, & H. Lacoste (Noordwijk: ESA), 81.1
Wang, Y.-M., Pick, M., & Mason, G. M. 2006, ApJ, 639, 495
Wang, Y.-M., & Sheeley, N. R., Jr. 2002, ApJ, 575, 542
Yashiro, S., Gopalswamy, N., Akiyama, S., Michalek, G., & Howard, R. A. 2005, J. Geophys. Res., 110, 10.1029/2005JA011151
Yashiro, S., Gopalswamy, N., Cliver, E. W., Reames, D. V., Kaiser, M. L., & Howard, R. A. 2004, in ASP Conf. Ser. 325, The *Solar-B* Mission and the Forefront of Solar Physics, ed. T. Sakurai, & T. Sekii (San Francisco: ASP), 401